A design and experimental verification methodology for an energy harvester skin structure

2011 Smart Mater. Struct. 20 057001

(http://iopscience.iop.org/0964-1726/20/5/057001)

Smart Mater. Struct. **20** (2011) 057001 (9pp) doi:10.1088/0964-1726/20/5/057001

TECHNICAL NOTE

A design and experimental verification methodology for an energy harvester skin structure

Soobum Lee[1] **and Byeng D Youn**[2,3]

[1] Department of Aerospace and Mechanical Engineering, University of Notre Dame, Notre Dame, IN 46545, USA
[2] School of Mechanical and Aerospace Engineering, Seoul National University, Seoul 151-742, Republic of Korea

E-mail: bdyoun@snu.ac.kr

Received 2 November 2010, in final form 9 March 2011
Published 30 March 2011
Online at stacks.iop.org/SMS/20/057001

Abstract
This paper presents a design and experimental verification methodology for energy harvesting (EH) skin, which opens up a practical and compact piezoelectric energy harvesting concept. In the past, EH research has primarily focused on the design improvement of a cantilever-type EH device. However, such EH devices require additional space for proof mass and fixture and sometimes result in significant energy loss as the clamping condition becomes loose. Unlike the cantilever-type device, the proposed design is simply implemented by laminating a thin piezoelectric patch onto a vibrating structure. The design methodology proposed, which determines a highly efficient piezoelectric material distribution, is composed of two tasks: (i) topology optimization and (ii) shape optimization of the EH material. An outdoor condensing unit is chosen as a case study among many engineered systems with harmonic vibrating configuration. The proposed design methodology determined an optimal PZT material configuration on the outdoor unit skin structure. The designed EH skin was carefully prototyped to demonstrate that it can generate power up to 3.7 mW, which is sustainable for operating wireless sensor units for structural health monitoring and/or building automation.

(Some figures in this article are in colour only in the electronic version)

1. Introduction

Research on energy harvesting (EH) has aimed to construct self-powered portable or wireless electrical devices (e.g., global positioning systems, wireless sensors) that use ambient, otherwise wasted, energy. As a result of the substantial research conducted in this field over the last two decades, current state-of-the-art devices can generate enough electrical power to operate wireless sensor nodes [1–3]. This EH technology is in high demand because wireless sensors are increasingly used in the areas of PHM (prognostics and health management) and/or building automation, and batteries can be troublesome due to their limited lifespan and high replacement cost ($80–$500 including labor [4]), especially when sensors are remotely installed. This issue has motivated the rapid growth of the EH field.

Vibration is one of the most available ambient energy forms found in civil structures, machines, and the human body, as listed by Roundy *et al* [5]. Among several energy conversion principles, piezoelectricity is known to be the most efficient energy conversion approach and the simplest and most practical means of conversion [6–8]. Among various kinds of piezoelectric material (e.g., PZT (lead zirconate titanate), ZnO (zinc oxide), and PVDF (polyvinylidene difluoride)), PZT is known to possess the best conversion efficiency [8].

Many researchers have studied piezoelectric energy harvesters utilizing ambient energy sources from machinery

[3] Author to whom any correspondence should be addressed.

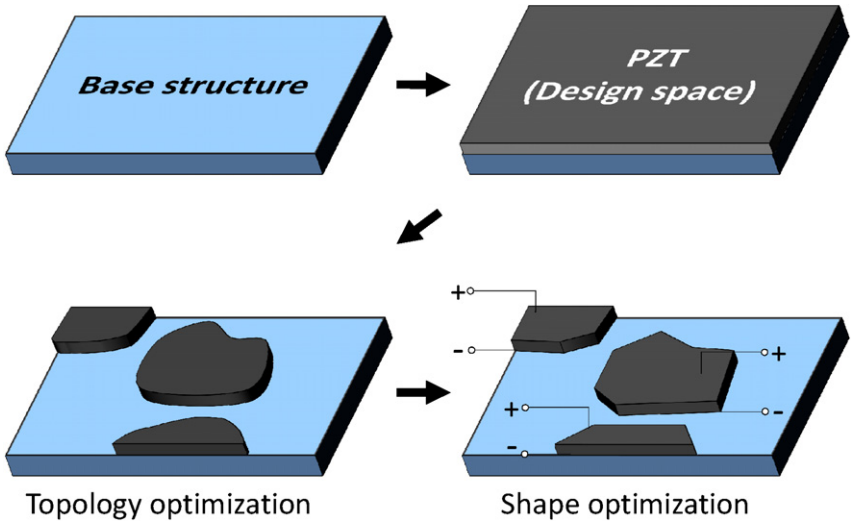

Figure 1. Design methodology for EH skin.

and human movement. Elvin *et al* [9] proposed a self-powered damage detection system for a construction site using PVDF: a time varying load from a roller cart that can generate sufficient mechanical strains for EH. Nuffer and Bein [10] discussed a health monitoring system for vehicles using wireless sensors operated by a piezoelectric energy harvester. Other case studies of EH from vehicle engine vibration and bridge vibration can be found on the AmbioSystems website [11]. Granstrom *et al* [12] developed a piezoelectric polymer backpack strap that generated electrical energy from the oscillating tension in the strap during walking. Leland *et al* [13] mounted an EH device on a wooden staircase and generated electricity from vibrations in the staircase to obtain around 30 μW. Shoe-mounted EH is another example of EH that utilizes human movement, in this case generating electricity through pressure by heel strikes [14, 15].

The design studies of piezoelectric EH include the design of mechanical characteristics (shape, location, material) and electric circuits. Some researchers have found that a trapezoidal cantilever shape is more efficient than a rectangular cantilever shape because of a uniformly large strain at every point on the beam surface [6, 16, 17]. Zheng *et al* [18] proposed a unique topology optimization method for an optimal piezoelectric EH cantilever design by maximizing an energy conversion factor. But, as Silva [19] discussed, Zheng *et al*'s work had limitations, in that it included consideration of only a static load and simplified electric circuitry. Erturk and Inman [20] pointed out several other oversimplified and incorrect physical assumptions from previous publications, such as an incorrect formulation for piezoelectric coupling, the use of low-fidelity models, and incorrect base motion modeling, and addressed these problems with improved models and examples. Recently, Rupp *et al* [21] developed a topology optimization method to design a multilayer, shell-type piezoelectric EH system. In their work the optimal external resistance value was simultaneously found by treating it as a design variable.

Piezoelectric material should be selected appropriately considering the vibration environment (vibration amplitude, temperature) and the required energy level of the harvester. Kim *et al* [22] summarized various kinds of piezoelectric materials and compared their energy conversion performances, operating temperature ranges, and modes to be utilized (e.g., d_{31}, d_{33}). Shen *et al* [23] experimentally compared the EH performance of three kinds of piezoelectric materials (piezoelectric ceramic [PZT], fiber, and polymer) and verified that PZT shows the best performance. Recent studies on piezoelectric EH devices are well summarized in review articles [17, 24, 25].

Most EH investigations have focused on piezoelectric EH devices such as a cantilever EH device. However, this type of EH device has some drawbacks from a practical point of view. First, the cantilever EH device requires extra space for a bulky proof mass and additional clamping part. Second, the cantilever EH device must be protected from dirt, moisture, and other environmental dangers. Therefore, it is usually suggested that the cantilever EH device be kept inside a case. Third, a great deal of vibration energy may be lost due to loosened clamping conditions after a long-time vibration. The disadvantages of the cantilever design have motivated the proposition of a compact and practical EH design called EH skin. In the EH skin, thin piezoelectric patches are directly attached onto a vibrating shell structure to harvest electric power. The direct attachment of thin piezoelectric patches is a well-known method for vibration control [26, 27] and nondestructive structural health monitoring [28]. However, to the best of our knowledge, there has been no systematic design approach for use of this direct attachment as an energy harvester. Therefore, a design and experimental verification methodology for the EH skin will be proposed in this paper.

The following sections will explain in detail the proposed design methodology for the EH skin (section 2) and experimental performance verification for an EH skin prototype (section 3).

2. Design methodology for energy harvesting skin

This section explains the proposed design methodology for the EH skin (see figure 1), which includes two main subtasks:

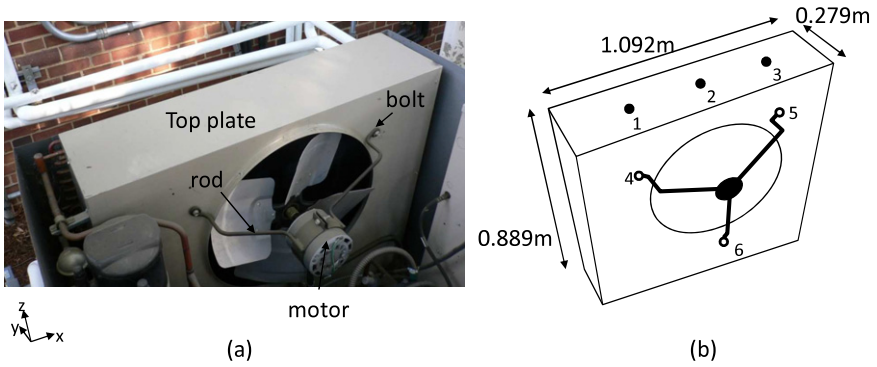

Figure 2. Outdoor condensing unit: (a) front view, (b) dimensions and data measurement points.

Table 1. Harmonic vibration measurement at excitation frequency ($f_e = 59.08$ Hz).

Point index	$z(g)$	Point index	x	y	z
1	4.22	4	0.18	0.69	0.18
2	0.25	5	0.20	0.49	0.31
3	1.13	6	0.04	0.11	0.16

(i) topology optimization (TO) and (ii) shape optimization (SO) of the EH skin. In the TO step, the topological distribution of piezoelectric material is found for effective energy harvesting. The material distribution found in this step, however, may be difficult to fabricate at the laboratory level. SO is therefore performed to fill the lack of manufacturability in the TO step.

Because the proposed design method uses computer simulation, a valid FE model on a vibrating engineered system should be prepared. The harvester design will be done using this valid FE model, and the calibrated material properties for PZT-5A [29] will be used. A case study on the valid FE model construction is briefly explained in the following section.

2.1. FE modeling of a vibrating skin structure—outdoor unit

The FE model for an outdoor unit (a cooler condensing unit manufactured by Bohn [30]), found on the campus of the University of Maryland (figure 2), is constructed and validated in this section. This kind of outdoor unit is widely available around buildings, and provides excellent vibration with a relatively high vibration level. Usually this kind of unit has harmonic vibration due to imbalance in the motor. The top plate of the outdoor unit was chosen as a design space for the EH skin due to its relatively high vibration level.

The harmonic vibration of the unit—the excitation (at points 4–6) and the plate response signals (points 1–3 in figure 2)—was measured. From the six points the average harmonic excitation frequency was measured as $f_e = 59.08$ Hz. Table 1 shows the averaged vibration amplitudes at each point.

The amplitude components for points 4–6 (see figure 2(b)) were used as the input loading condition in the FE model. Figure 3 shows this FE model with the fixed boundary conditions. The FE model was constructed using the

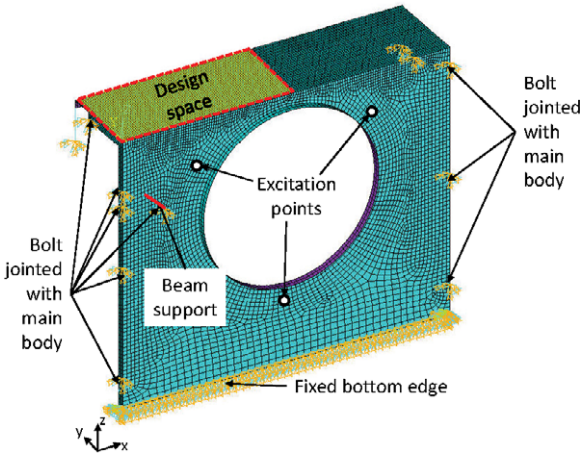

Figure 3. Fixed boundary conditions and excitation points.

Table 2. Calibration result on response.

	Amplitude (g)	
Point index	Measurement	Simulation
1	4.22	3.53
2	0.25	0.28
3	1.13	1.70

SHELL181 element in ANSYS, and calibrated to have the harmonic response close to the measured response. Through the calibration, the overall behavior or the simulated harmonic responses matched well with the measured responses—two local peaks at points 1 and 3 (as shown in table 2). The details on the model calibration study are explained in [31].

2.2. Design optimization of EH skin

Based on the calibrated model for the vibrating skin structure, the design task for finding an optimal piezoelectric material distribution as well as optimal external resistance was performed so as to yield maximum power generation. As introduced in the beginning of section 2, the topology optimization and shape optimization techniques were performed consecutively.

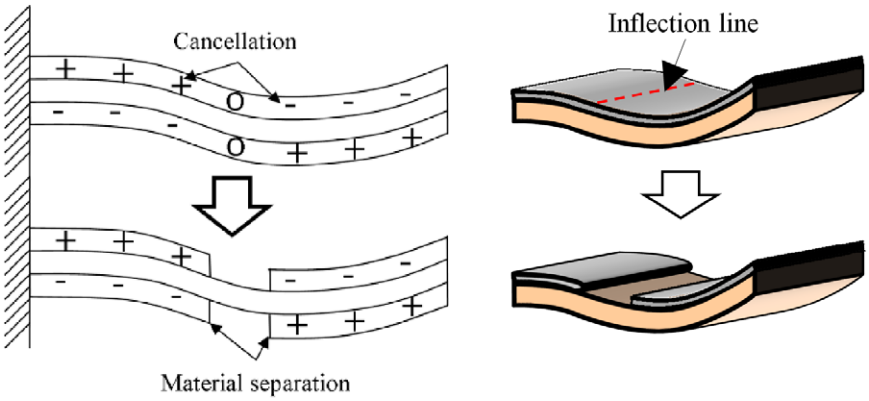

Figure 4. Minimization of cancelation effect by eliminating the inflection line.

2.2.1. Topology optimization. In this step, a conceptual design optimization was performed to find an optimal topology of the PZT material. Initially a thin PZT layer covered the whole design space (as shown in the second step in figure 1), and the material distribution was conceptually found by eliminating some PZT material. The properties for PZT, shown in table 3, were taken from our previous calibration study [29]. The material properties of steel are also listed in the table. A patch had the dimensions $A_p = 72.4 \times 72.4$ mm^2, 0.19 mm thick, and both sides were laminated with nickel electrode. The design problem was defined to find the optimal PZT distribution subject to material constraint (seven PZT patches) due to cost limitation. The PZT patches were modeled using SOLID5 element in ANSYS, a 3D coupled-field solid element. The volt DOFs on the PZT top surface were coupled to represent the top electrode, and those on the interface with the outdoor unit plate were grounded to represent the bottom electrode.

The hard kill method [32–34] was chosen for this step. This method is one of the most widely used TO design methods due to its simplicity—at each iteration a preset number of elements is erased based on a certain criterion. The criterion is defined per each element, reflecting the change of design performances (e.g., objective and constraint functions) by eliminating the element. In this study a simple but logical criterion was introduced. Based on the fact that the higher in-plane strain ensured the larger voltage generation [35, 36] when 31 mode was utilized, the TO tried to eliminate the elements having low in-plane strain. The TO also considered the cancelation effect [21, 29, 37], referred to as voltage cancelation, due to different strain signs in one PZT material. Figure 4 shows an example of this effect from the second vibration mode of a cantilever. Voltage cancelation occurred in this mode due to different signs of mode-shape curvature. Obviously, this effect can be minimized by eliminating material around the inflection line, and the line can be detected based on the amount of in-plane strain; the strain amount is locally smaller around the inflection line because of the strain sign change near the line. In summary, the elements having relatively low in-plane strain will be eliminated. The eliminating criterion (α) for the TO is defined as the sum of the in-plane normal strain along each direction, or

$$\alpha = |\varepsilon_{xx} + \varepsilon_{yy}|. \tag{1}$$

Through the TO, the PZT material was distributed in the high-strain region without voltage cancelation. The optimization is terminated when the constraint on the PZT material is satisfied. The TO procedure is summarized in figure 5.

Even after the material constraint is satisfied (first diamond in figure 5), all the inflection lines may not be clearly eliminated. An additional inspection step (second diamond in figure 5) is therefore introduced for this purpose. The existence of inflection lines is checked by the phase angle of $\varepsilon_{xx} + \varepsilon_{yy}(\phi(\varepsilon_{xx} + \varepsilon_{yy}))$ for each element. It is judged that an inflection line exists if $|\phi_j(\varepsilon_{xx} + \varepsilon_{yy}) - \phi_k(\varepsilon_{xx} + \varepsilon_{yy})| > \phi_0$, where j and k ($j \neq k$) are the element index in a segment and ϕ_0 is the threshold on phase difference. Usually there is a

Table 3. Material properties for steel and PZT-5A.

Material	Properties	Value
Steel	Density	7889 kg m^{-3}
	Poisson's ratio	0.3
	Young's modulus	$2.00 \times 10^{+11}$ Pa
PZT-5A	Density	7171 kg m^{-3}
	Compliance matrix component	
	s_{11}	1.64×10^{-11} m^2 N^{-1}
	s_{12}	-5.74×10^{-12} m^2 N^{-1}
	s_{13}	-7.22×10^{-12} m^2 N^{-1}
	s_{33}	1.88×10^{-11} m^2 N^{-1}
	s_{44}	4.75×10^{-11} m^2 N^{-1}
	s_{66}	4.43×10^{-11} m^2 N^{-1}
	Piezoelectric coupling coeff.	
	d_{31}	-1.71×10^{-10} C N^{-1}
	d_{33}	3.74×10^{-10} C N^{-1}
	d_{15}	5.84×10^{-10} C N^{-1}
	Relative permittivity at constant strain	
	ε_{11}	916
	ε_{33}	830

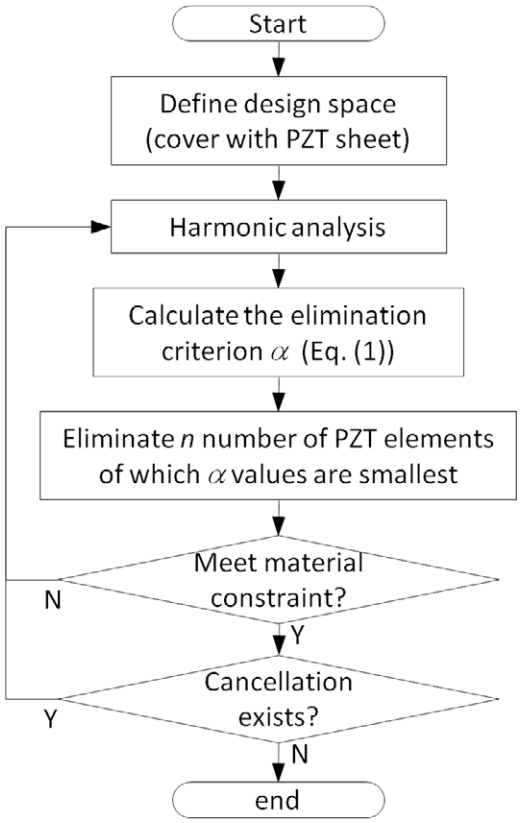

Figure 5. Topology optimization procedure.

significant phase change (e.g., $\phi_0 = 180°$) if an inflection line exists.

Figure 6 shows the TO procedure using the hard kill method. At every iteration n (=10) number of elements were removed to find the final PZT distribution. After 197 iterations the TO procedure stopped and no inflection line was detected. The procedure found three segments around point 1 (see figure 2), along the long lower edge, and locally at the left edge.

2.2.2. Shape optimization. The SO step was performed to supplement the TO result for the following reasons: (i) element elimination is based on in-plane strain, not exactly on the output power, and (ii) manufacturability is not considered in the TO. Usually, cutting a PZT sheet into curved shapes is costly because it requires a high-precision cutting tool. Therefore each segment was reconstructed as a polygon. The smallest segment on the left in the TO result was discarded due to its relatively negligible size and power output. Three cases of model parameterization were studied to find: (i) the optimal location of two rectangular PZT segments, (ii) the optimal rectangle segment shapes, and (iii) the optimal polygon segment shapes (octagon for center, hexagon for bottom segment).

The initial design for SO was set to be identical for all the three cases, as the closest rectangles to the TO result. Minimum cutting labor was considered in case (i) where six patches were located at the center, while one patch was cut into two pieces to form a long rectangle at the bottom. Case (ii) dealt with the shape optimization of two rectangles where a total of seven design variables were involved. In case (iii) each segment was assumed to be a polygon (an octagon for the center, and a hexagon for the bottom segment). The x and y coordinates of each vertex were defined as design variables, 24 in total. The model parameterization was done using the morphing technique supported by Hypermesh [38].

In the SO step, an external resistor was implemented between the top and bottom electrode of each PZT segment, using CIRCU94 element in ANSYS. The resistance sweep test was done for the initial design using FE simulation, and the optimal resistance values for each segment (R_j^0, $j = 1, 2$) were 1750 and 10 575 Ω for the center and bottom segments, respectively.

The following SO formulation was used to maximize the power generation under the area and strain constraints as:

$$\begin{aligned} &\max \sum_j P_j(dv_i) \\ &\text{s.t.} \sum_j A_j(dv_i) \leqslant A_0 \\ &\max(\varepsilon_{\text{von}}) \leqslant \varepsilon_{\text{yield}} \\ &lb_i \leqslant dv_i \leqslant ub_i \end{aligned} \tag{2}$$

where P_j is the power from the jth segment ($j = 1, 2$), dv_i is the ith design variable with its bounds (lb_i, ub_i), ε_{von} is the

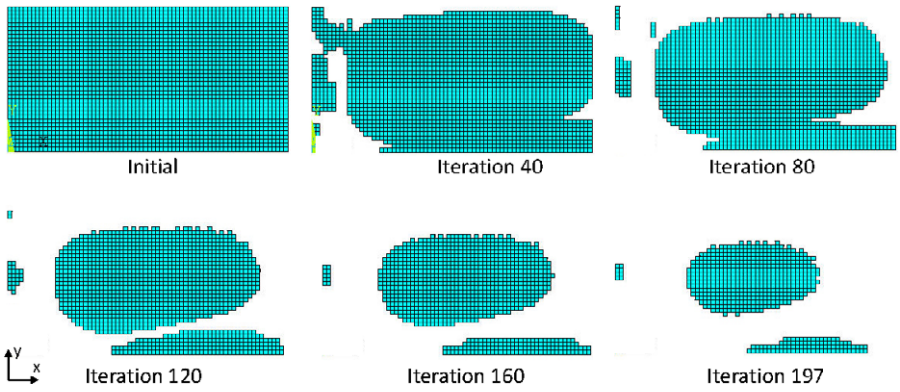

Figure 6. Topology optimization history.

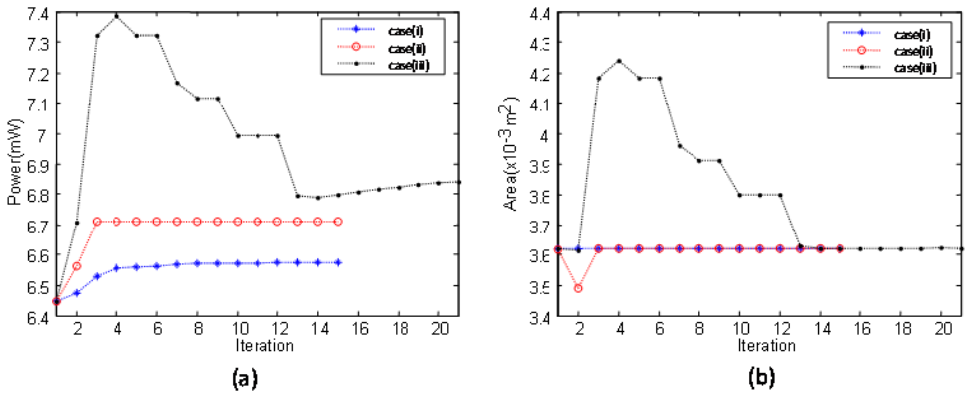

Figure 7. Optimization history (a) objective function, (b) constraint on PZT area.

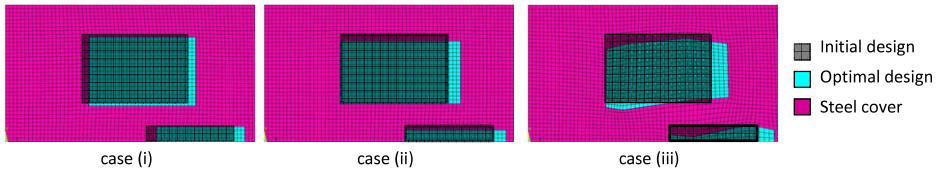

Figure 8. Shape change for three cases.

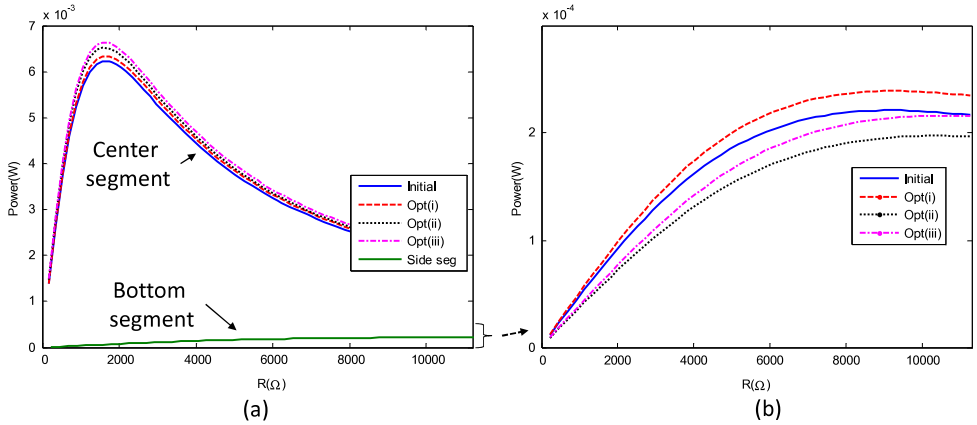

Figure 9. Resistance sweep test for initial and optimal model (a) for both segments, (b) for bottom segment.

maximum von Mises strain of the PZT material, $\varepsilon_{\text{yield}}$ is the allowable strain of the PZT, which is set to 500 μ [17]. A_0 was set to $7A_p$ ($A_p = 72.4 \times 72.4$ mm^2). In this study the bounds for each design variable were set to ± 2.5 cm from their initial values. During the SO the material topology does not change and the number of segments is maintained.

The SO results for all the three cases are summarized in figures 7 and 8. Case (iii) yielded more power than any other case due to the larger degrees of freedom for design improvement. The SO for the three cases required 15, 15, and 21 design optimization iterations, respectively, and the constraints were satisfied for all the cases. The power increase through the SO was marginal (6.6% in case (iii)), which indicates the excellent performance of the proposed TO strategy in section 2.2.1.

Figure 8 shows the design change through the SO. As explained earlier, the morphing technique enabled smooth design perturbation. In all the cases, the design was shifted right and downward. The SO step completes the entire design procedure and produces a manufacturable EH design output.

Figure 9 shows the power outputs for all the cases as a function of resistance (R_j). The peak value of the power is listed in table 4. One can observe that the power output from the center segment is significantly larger than the bottom segment for all the cases.

3. Experimental verification of an optimal EH skin

3.1. Energy harvesting skin prototype

For prototype manufacturing and verification, we chose the center segment from case (i) due to its larger power output and ease of manufacturing—this case does not require additional cutting of the patches. The center segment in figure 8 (case (i)) was prototyped using six PZT patches.

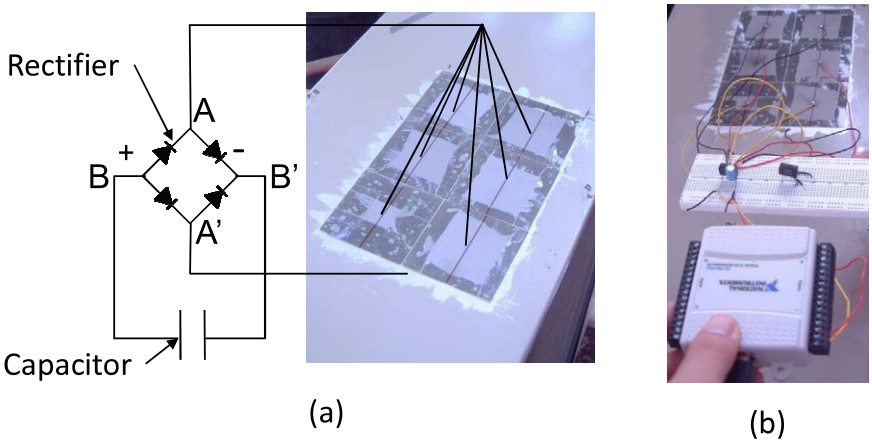

Figure 10. Power measurement for EH skin (a) circuit diagram, (b) still cut for power measurement.

Table 4. Power output for each case.

	Power (mW)		
Case	Segment 1 (center)	Segment 2 (bottom)	Sum
Initial	6.236	0.212	6.448
(i)	6.347	0.226	6.573
(ii)	6.524	0.187	6.711
(iii)	6.640	0.201	6.841

The prototype is fabricated by attaching PZT patches using conductive epoxy. Conductive epoxy was electrically insulated from the outdoor top plate because the plate was covered with a layer of paint. The bottom electrode can be easily accessed through the widely spread epoxy. Special attention had to be paid, however, to prevent short circuitry between the top and bottom electrode because the 'paste' state epoxy may be squeezed out and reach the top electrode. To prevent this, transparent tape was attached along the edges of the top PZT surface before curing.

3.2. Power evaluation

The verification metric is the power generation from the EH skin, which was measured via a data acquisition and power calculation process. The six patches were connected parallel so that they electrically behaved as one big patch. That is, the six wires soldered at each top electrode were connected together to share the same voltage through the six top electrodes, and the wire soldered at epoxy layer was electrically connected to each bottom electrode. These two electrodes were linked to a rectifier and finally a capacitor (100 μF), where the electric charge accumulated. This circuit is shown in figure 10(a). The power was measured using an NI USB-6009 portable DAQ device (see figure 10(b)).

The voltage history is shown in figure 11. The power was estimated using the following equation:

$$P = \frac{E}{T} = \frac{1}{2T} C V(T)^2 \tag{3}$$

where P is the average power, E is electrical energy, T is charging time, C is capacitance, and $V(T)$ is the voltage accumulated by time T. The power was repeatedly measured (eight times) to yield the average value of 3.68 mW, as shown in table 5, which is about 58% of the simulation result (6.35 mW).

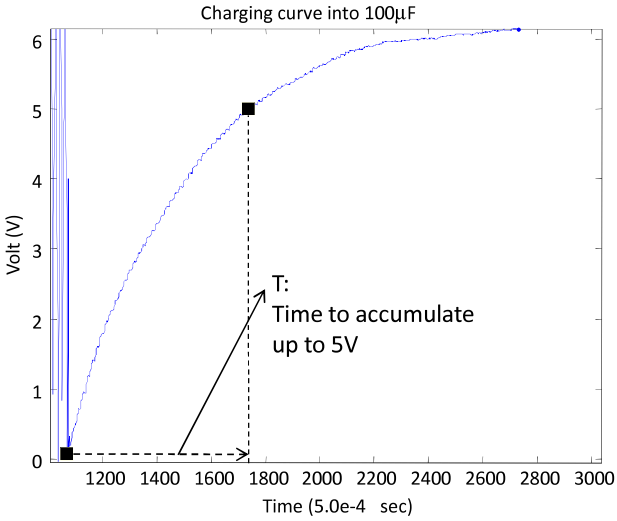

Figure 11. Power charging curve.

Table 5. Power measurement.

Measurement	Power (mW)
1	3.743
2	3.726
3	3.462
4	3.644
5	3.731
6	3.894
7	3.311
8	3.925
Average	3.677

3.3. Discussion

The power discrepancy between the simulation and experiment can primarily be attributed to some of the following factors:

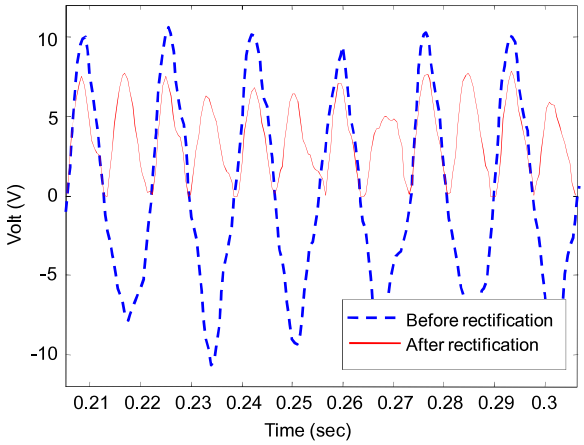

Figure 12. Open circuit voltage before and after rectification.

- Imperfect bonding condition of PZT patches.
- Voltage drop through the electronics, especially a rectifier.
- Possible partial damage or degradation in PZT patches.

The simulation assumes perfect bonding of PZT patches and no voltage drop in the electronics. However, first, perfect bonding is never possible in a real-world setting. It is known that as the size of the PZT patches grows, the effect of bonding becomes much more significant. Considering the relatively large PZT patches in the prototype, the bonding condition is thought to be one of the main factors for the discrepancy. Second, a significant voltage drop through the electronics, especially the rectifier, may cause the discrepancy. The voltage before rectification (A–A′) and after rectification (B–B′ in figure 10(a)) was recorded as shown in figure 12, where a significant voltage drop was observed (about 30%). Even though we believe this factor can be overcome by replacing the rectifier used in the circuit with a high-quality rectifier, this part needs more study. Despite the difference in power generation between the simulation and the test, however, a significant power level has been achieved. We believe this work illustrates the greater capabilities of the EH skin from two primary perspectives:

(i) Sustainable and relatively high-power generation to operate low-power electronics, such as wireless sensors used for health monitoring [39] and/or building automation [40].
(ii) Compact EH design to require no need of fixture and proof mass.

4. Conclusion

This paper presented a design and experimental verification methodology for the EH skin. The EH skin design was optimized through the two main design steps: TO and SO. Based on the calibrated FE model for a vibrating system (the outdoor unit), the optimal PZT material distribution was conceptually found using the hard kill method in the TO step. The eliminating criterion (α) was proposed to iteratively remove PZT materials (i) having low in-plane strain, and (ii) along inflection lines for cancelation effect minimization. The SO step was consecutively performed to finalize the EH skin design. In the SO step, the FE model was parameterized using the morphing technique in Hypermesh. The optimized design was fabricated on the top plate of the outdoor unit, and the performance was verified.

The characteristics and limitations of the proposed design method due to the direct attachment may include:

(i) The design task was done based on the assumption that the vibrating configuration of the structure (e.g., excitation harmonic frequencies, resonant frequencies of outdoor unit) is maintained.
(ii) If the EH skin is composed of multiple segments, the way to simplify electric wiring has to be sought.

For the first problem, even though the design method does not actively perform frequency tuning process, the vibration mode utilized for EH is chosen whose resonant frequency (60.38 Hz) is closer to the harmonic frequency (59.08 Hz). By doing this, our prototype could obtain sufficient power (3.68 mW) for operating a three-axis accelerometer. For the second problem, we may use an advanced wiring technique such as conductive tape or silver pen, to avoid complicated wiring and maintain design compactness.

In this study we calibrated the FE model for an engineering system (outdoor unit) in terms of vibration amplitude. Dynamic strain sensors may be considered in a future study so that one can calibrate the FE model more accurately in terms of strain, because dynamic strain is a structural response directly related to PZT power generation. The future plan also includes (i) the development of high-efficiency EH skin which may utilize multiple vibration modes, (ii) its practical application to aircrafts or ground transportation where vibrating skins are commonly found, and (iii) a successful operation of a wireless sensor network for structural health monitoring.

Acknowledgments

This work was partially supported by the National Research Foundation of Korea Grant funded by the Korean Government (NRF-2009-352-D00007) and by the SNU-IAMD. The facility support by the Center for Environmental Energy Engineering (CEEE) at the University of Maryland is greatly appreciated. We also thank Mr Matthieu Giraud for assisting us with related measurements.

References

[1] Bai H, Atiquzzaman M and Lilja D 2004 Wireless sensor network for aircraft health monitoring *BroadNets' 04: Proc. 1st Int. Conf. on Broadband Networks (San Jose, CA, Oct. 2004)* ed B Werner (Los Alamitos, CA: IEEE Computer Society) pp 748–50
[2] Roundy S, Wright P K and Rabaey J 2003 A study of low level vibrations as a power source for wireless sensor nodes *Comput. Commun.* **26** 1131–44
[3] Park G, Rosing T, Todd M D, Farrar C R and Hodgkiss W 2008 Energy harvesting for structural health monitoring sensor networks *J. Infrastruct. Syst.* **14** 64–79

[4] *ITP Sensors and Automation: Low-Cost Vibration Power Harvesting for Wireless Sensors* US Department of Energy Energy Efficiency and Renewable Energy (cited 2008 Dec. 4) available from http://www1.eere.energy.gov/industry/sensors_automation/pdfs/kcf_vibrationpower.pdf

[5] Roundy S, Wright P K and Rabaey J M 2004 *Energy Scavenging for Wireless Sensor Networks: With Special Focus on Vibrations* (Berlin: Springer)

[6] Glynne-Jones P, Beeby S P and White N M 2001 Towards a piezoelectric vibration-powered microgenerator *IEE Sci., Meas. Technol.* **148** 68–72

[7] Sterken T, Baert K, Van Hoof C, Puers R, Borghs G and Fiorini P 2004 Comparative modelling for vibration scavengers *Proc. IEEE Sensors 2004 (Vienna, Oct. 2004)* ed D Rocha, P M Sarro and M J Vellekoop pp 1249–52

[8] Silk M G 1984 *Ultrasonic Transducers for Nondestructive Testing* (Bristol: Hilger)

[9] Elvin N, Elvin A and Choi D H 2003 A self-powered damage detection sensor *J. Strain Anal. Eng. Des.* **38** 115–24

[10] Nuffer J and Bein T 2006 Applications of piezoelectric materials in transportation industry *TRANSFAC '06: Proc. Global Symp. on Innovative Solutions for the Advancement of the Transport Industry (San Sebastian, Oct. 2006)* ed J Goñi, G Lilly, I Inzunza, E Erauzkin, C Mereveille, C Elizetxea, N Markaide and B Mishra

[11] Anton S R and Sodano H A 2007 A review of power harvesting using piezoelectric materials (2003–2006) *Smart Mater. Struct.* **16** R1–21

[12] Granstrom J, Feenstra J, Sodano H A and Farinholt K 2007 Energy harvesting from a backpack instrumented with piezoelectric shoulder straps *Smart Mater. Struct.* **16** 1810–20

[13] Leland E S, Lai E M and Wright P K 2004 A self-powered wireless sensor for indoor environmental monitoring *Proc. WNCG Conf. (Austin, TX, Oct. 2004)*

[14] Shenck N S and Paradiso J A 2001 Energy scavenging with shoe-mounted piezoelectrics *IEEE MICRO* **21** 30–42

[15] Mateu L and Moll F 2005 Optimum piezoelectric bending beam structures for energy harvesting using shoe inserts *J. Intell. Mater. Syst. Struct.* **16** 835–45

[16] Goldschmidtboeing F and Woias P 2008 Characterization of different beam shapes for piezoelectric energy harvesting *J. Micromech. Microeng.* **18** 104013

[17] Roundy S, Leland E S, Baker J, Carleton E, Reilly E, Lai E, Otis B, Rabaey J M, Wright P K and Sundararajan V 2005 Improving power output for vibration-based energy scavengers *IEEE Pervasive Comput.* **4** 28–36

[18] Zheng B, Chang C J and Gea H C 2009 Topology optimization of energy harvesting devices using piezoelectric materials *Struct. Multidiscip. Optim.* **38** 17–23

[19] Silva E C N 2009 Comment on 'Topology optimization of energy harvesting devices using piezoelectric materials' *Struct. Multidiscip. Optim.* **39** 337–8

[20] Erturk A and Inman D J 2008 Issues in mathematical modeling of piezoelectric energy harvesters *Smart Mater. Struct.* **17** 065016

[21] Rupp C J, Evgrafov A, Maute K and Dunn M L 2009 Design of piezoelectrc energy harvesting systems: a topology optimization approach based on multilayer plates and shells *J. Intell. Mater. Syst. Struct.* **20** 1923

[22] Kim H, Tadesse Y and Priya S 2009 Piezoelectric energy harvesting *Energy Harvesting Technologies* ed S Priya and D J Inman (New York: Springer) pp 9–16

[23] Shen D, Choe S Y and Kim D J 2007 Analysis of piezoelectric materials for energy harvesting devices under high-g vibrations *Japan. J. Appl. Phys.* **46** 6755–60

[24] Sodano H A, Inman D J and Park G 2004 A review of power harvesting from vibration using piezoelectric materials *Shock Vib. Digest* **36** 197–206

[25] Anton S R and Sodano H A 2007 A review of power harvesting using piezoelectric materials (2003–2006) *Smart Mater. Struct.* **16** R1

[26] Lam K Y and Ng T Y 1999 Active control of composite plates with integrated piezoelectric sensors and actuators under various dynamic loading conditions *Smart Mater. Struct.* **8** 223–37

[27] Song G, Sethi V and Li H N 2006 Vibration control of civil structures using piezoceramic smart materials: a review *Eng. Struct.* **28** 1513–24

[28] Park G, Sohn H, Farrar C R and Inman D J 2003 Overview of piezoelectric impedance-based health monitoring and path forward *Shock Vib. Digest* **35** 451–64

[29] Lee S, Youn B D and Jung B C 2009 Robust segment-type energy harvester and its application to a wireless sensor *Smart Mater. Struct.* **18** 095021

[30] Bohn: The Cold Standard (cited 2009 8 Sept.) available from http://www.thecoldstandard.com/

[31] Lee S, Youn B D and Giraud M 2010 Designing energy harvesting skin structure utilizing outdoor unit vibration *IDETC: Proc. Int. Design Engineering Technical Conferences (Montreal, Aug. 2010)*

[32] Xie Y M and Steven G P 1997 *Evolutionary Structural Optimization* (Berlin: Springer)

[33] Xie Y M and Steven G P 1996 Evolutionary structural optimization for dynamic problems *Comput. Struct.* **58** 1067–73

[34] Kim H, Querin O M, Steven G P and Xie Y M 2000 A method for varying the number of cavities in an optimized topology using evolutionary structural optimization *Struct. Multidiscip. Optim.* **19** 140–7

[35] Chen S N, Wang G J and Chien M C 2006 Analytical modeling of piezoelectric vibration-induced micro power generator *Mechatronics* **16** 379–87

[36] Lu F, Lee H P and Lim S P 2004 Modeling and analysis of micro piezoelectric power generators for micro-electromechanical-systems applications *Smart Mater. Struct.* **13** 57–63

[37] Erturk A, Tarazaga P A, Farmer J R and Inman D J 2009 Effect of strain nodes and electrode configuration on piezoelectric energy harvesting from cantilevered beams *J. Vib. Acoust.* **131** 011010

[38] HyperWorks 2008 Altair Engineering Inc. http://www.altairhyperworks.com

[39] Arms S W, Townsend C P, Churchill D L, Galbreath J H and Mundell S W 2005 Power management for energy harvesting wireless sensors *Proc. SPIE* **5763** 267–75

[40] Echoflex 43-160 Wireless Self Powered Photo Sensor (cited 2010 5 March) available from http://www.energyharvestingjournal.com/articles/mobile-kinetic-energy-harvester-00001457.asp